Last Glacial Maximum over China: Sensitivities of climate to paleovegetation and Tibetan ice sheet

Dabang Jiang and Huijun Wang

State Key Laboratory of Numerical Modeling for Atmospheric Sciences and Geophysical Fluid Dynamics (LASG), Institute of Atmospheric Physics, Chinese Academy of Sciences, Beijing, China

Helge Drange

Nansen Environmental and Remote Sensing Center, Bergen, Norway

Xianmei Lang

State Key Laboratory of Numerical Modeling for Atmospheric Sciences and Geophysical Fluid Dynamics (LASG), Institute of Atmospheric Physics, Chinese Academy of Sciences, Beijing, China

Received 5 February 2002; revised 3 October 2002; accepted 3 October 2002; published 6 February 2003.

[1] With the boundary conditions appropriate for the Last Glacial Maximum (LGM), including ice sheets, sea surface temperatures, sea-ice distribution, atmospheric CO_2 concentration, the Earth's orbital parameters, topography, and coastline, the atmospheric general circulation model of the Institute of Atmospheric Physics (IAP-AGCM) computes colder and drier conditions than for present day. Global annual-average surface temperature decreased by 5.3°C, and terrestrial precipitation was down by 29%. It is shown that IAP-AGCM LGM simulation compares favorably to results from other AGCMs, and/but generally shows a weak terrestrial cooling when compared to paleoclimatic reconstructions in tropics. The 21 ka (ka: thousands of years ago) vegetation reconstruction is introduced into the model to study the regional climate response to the changes in vegetation and associated soil characteristics over China. The additional cooling due to these two changes reduces, to a certain degree, the model-data discrepancies. In addition, under the precondition of continental ice existing over part of the Tibetan Plateau at the LGM, the authors examine the regional climate response to the continental ice. It follows that the glacial-age environment over the Tibetan Plateau is a very important factor for 21 ka climate simulation in East Asia. *INDEX TERMS:* 3309 Meteorology and Atmospheric Dynamics: Climatology (1620); 3322 Meteorology and Atmospheric Dynamics: Land/atmosphere interactions; 3344 Meteorology and Atmospheric Dynamics: Paleoclimatology; *KEYWORDS:* last Glacial Maximum, climate, paleovegetation, Tibetan ice sheet

Citation: Jiang, D., H. Wang, H. Drange, and X. Lang, Last Glacial Maximum over China: Sensitivities of climate to paleovegetation and Tibetan ice sheet, *J. Geophys. Res.*, *108*(D3), 4102, doi:10.1029/2002JD002167, 2003.

1. Introduction

[2] Documenting the characteristics of past climates and understanding the causes of climatic change are major challenges for studies of the earth system [*Kutzbach et al.*, 1998]. Even if models could simulate today's climate perfectly, this would not guarantee an accurate simulation of climate change [*Joussaume et al.*, 1999]. Therefore, the ability to correctly simulate past climates bears directly on whether we can confidently forecast future climates [*Kohfeld and Harrison*, 2000]. If climate models can successfully reproduce paleoclimatic characteristics in different historical periods, the confidence in predicting future climate changes will certainly increase.

0148-0227/03/2002JD002167$09.00

[3] The Last Glacial Maximum (LGM) has been chosen as one of the two focal periods (the other is the mid-Holocene) by the Paleoclimate Modeling Intercomparison Project (PMIP) [*Joussaume and Taylor*, 1995] because of a great climate difference from the present day (PD) and a variety of reconstructed data available for this period. Previous modeling studies of the LGM have indicated that the climate differences between this period and PD are mainly a response to the presence of northern hemisphere ice sheets, more extensive sea ice, colder glacial-age sea surface temperatures (SSTs), and a lower CO_2 concentration, and some of the major 21 ka climate characteristics have been successfully reproduced [e.g., *Broccoli and Manabe*, 1987; *COHMAP members*, 1988; *Dong et al.*, 1996; *Dong and Valdes*, 1998; *Kutzbach et al.*, 1998; *Pinot et al.*, 1999; *Yu et al.*, 2001a]. Recently, *Broccoli* [2000] emphasized the use of coupled ocean-atmosphere general circulation models, and

Yin and Battisti [2001] indicated the importance of the tropical SSTs distribution.

[4] However, discrepancies between proxy estimates and the integrations of AGCMs with either fixed SSTs or slab ocean models still exist, and cannot even be reconciled in some regions. For the LGM, the disagreements between simulated and observed climates may reflect inadequacies in the formulation of the model, in the specification of prescribed boundary conditions, or in the coverage and interpretation of the paleoenvironmental data [*Kutzbach et al.*, 1998].

[5] It has been amply documented that vegetation plays an important role in the current climate system [e.g., *Sellers et al.*, 1986]. However, AGCMs (some coupled to a slab ocean) used to simulate the LGM climate are typically run with modern vegetation distribution. Recently, simulations of the LGM climate using the 21 ka vegetation reconstruction were performed by *Crowley and Baum* [1997] and *Wyputta and McAvaney* [2001]. Furthermore, *Kubatzki and Claussen* [1998] simulated the glacial climate with the coupled ECHAM-BIOME model, and *Levis et al.* [1999] examined the potential for vegetation feedbacks on the climate system at the LGM with a fully coupled climate-vegetation model GENESIS-IBIS. These pioneering studies show the important role of vegetation feedback on the LGM climate. Inclusion of ''realistic'' vegetation generally leads to additional cooling in some regions and reduces, to a certain degree, the disagreements between simulated climate and proxy estimates. Then, what is the role of paleovegetation feedback on the LGM climate over China?

[6] Scientists have studied the glacial-age environment over the Tibetan Plateau for a long time, but there is still no consensus. According to some research results [*Kuhle*, 1987, 1991; *Han*, 1991; *Liu et al.*, 1999], it is very possible that large volumes of continental ice were present over part of the Tibetan Plateau at the LGM. So, what is the potential influence of the above-mentioned continental ice on the LGM climate simulation in East Asia if it indeed existed at that period?

[7] In this study, four simulations are performed in order to assess the effect the above vegetation feedback and ice sheet have on the LGM climate. After describing the IAP-AGCM in section 2 and the experimental design in section 3, section 4 is devoted to the main LGM simulation. In section 5, two sensitivity experiments are represented to address the role of paleovegetation feedback over China and climate response to the continental ice over the Tibetan Plateau. The study is concluded in section 6.

2. Model

[8] The IAP-AGCM has been developed at the Institute of Atmospheric Physics under the Chinese Academy of Sciences. It is a global grid point model with $5^\circ \times 4^\circ$ (longitude by latitude) horizontal resolution. The model has nine levels unevenly spaced in the vertical direction with the upper model boundary at 10 hPa. The operational design of the model dynamics was completed by *Zhang* [1990]. The model uses a finite difference scheme that conserves the ''available'' energy in the C-grid spherical coordinate system [*Zeng et al.*, 1987]. The moisture transport is predicted by the multidimensional positive finite advection transport algorithm of *Smolarkiewicz and Grabowski* [1990]. This scheme is nonoscillatory with small diffusion so it predicts a positive definite quantity with high accuracy. The model simulates dry and moist convective adjustments, and shallow and penetrative cumulus convection. Shallow cumulus convection is parameterized according to *Albrecht et al.* [1986]. The scheme is an effective mass flux representation of convective heat and moisture fluxes. Penetrative cumulus convection is simulated by the *Arakawa and Schubert* [1974] scheme in the implementation of *Lord* [1978] and *Lord et al.* [1982]. Precipitation is produced by penetrative convection and large-scale condensation. The large-scale precipitation forms as a result of local supersaturation under stable conditions. The amount of cloud is diagnostically determined from the relative humidity, vertical velocity, atmospheric stability, and convective precipitation rate, following the *Slingo* [1987] approach. In the model, convective cloud, stratiform cloud, low-level marine stratus, and stratocumulus cloud associated with temperature inversions are treated. Clouds may form everywhere except in the surface layer to prevent the development of excessive low cloudiness. Both solar and terrestrial radiation schemes are adopted from the U.S. National Center for Atmospheric Research's (NCAR'S) Community Climate Model version 1 (CCM1), which is described in detail by *Kiehl et al.* [1987]. The gravity wave-drag scheme is that of *Palmer et al.* [1986]. The land surface process scheme follows that of *Liang* [1996]. It consists of a two-layer soil model, a surface energy balance model, and a primitive plant canopy model coupled with a planetary boundary layer model. The land surface vegetation is grouped into 10 categories. For the IAP-AGCM performance for PD climate, see *Bi* [1993] for an overview.

3. Boundary Conditions and Experimental Design

3.1. Boundary Conditions for the LGM

[9] The Earth orbital parameters are modified to their 21 ka configuration according to *Berger* [1978], although this has only a minor effect on the LGM climate because these parameters are similar to the modern values with the phase of precession and eccentricity almost identical to the PD, and obliquity slightly less than the PD.

[10] We use ice sheets and topography data constructed by *Peltier* [1994] for the LGM. When the data is interpolated, i.e., changing horizontal resolution from $1^\circ \times 1^\circ$ to $5^\circ \times 4^\circ$, the ice sheet is present in the model when there are at least nine ice sheet grid points according to the Peltier data set within each model grid cell. In addition, because the 21 ka topographical height is averaged within 20 of the Peltier grid points, the data are smoother for mountain regions and slightly lower than the original. Furthermore, the coastline is defined by the topographical height. If it is above (below) 0, land (ocean) is assumed. Additional land points due to sea level lowering are given the same vegetation type as the neighboring land point(s). If both of the neighboring points are ocean points, they are given the most abundant vegetation type at the same latitude.

[11] The SSTs and sea-ice data from *CLIMAP Project members* [1981] are available for February and August only. To get monthly varying SSTs, a sinusoidal variation with

Table 1. Tabulation of the Boundary Conditions for the Present Day (PD) and Last Glacial Maximum

Time, ka	Earth's Orbital Parameters: Eccentricity	Obliquity	Longitude of Perihelion	CO_2 Concentration, ppmv	Ice Sheets, Topography and Coastline	SSTs, Sea Ice
0	0.016724	23.446°	102.039°	345	PD	PD
21	0.018994	22.949°	114.425°	200	*Peltier* [1994]	*CLIMAP Project members* [1981]

extremes in February and August is used. When sea ice occurs for both February and August, a permanent sea-ice cover is prescribed for all months. When there is sea ice in February (August) but not in August (February), sea-ice cover is assumed for November to March (May to September). The atmospheric CO_2 concentration at the LGM is set to 200 ppmv, a value based on ice core measurements [*Barnola et al.*, 1987; *Leuenberger and Siegenthaler*, 1992; *Raynaud et al.*, 1993]. All of the above data constitute the boundary conditions appropriate for the LGM recommended by PMIP [*Joussaume and Taylor*, 1995]. See Table 1 for a summary.

3.2. Experimental Design and Length of Runs

[12] Four numerical experiments have been performed, hereafter Exp1 to Exp4. The boundary conditions for each of the experiments are summarized in Table 2. Exp1 can be regarded as the control run and Exp2 as a PMIP-like simulation because the PMIP methodology in building the boundary conditions for the LGM stipulates taking the PD topography and adding to it the difference between LGM and PD to obtain a LGM elevation, not taking the absolute elevation values from the reconstruction [*Peltier*, 1994]. Similarly, IAP-AGCM uses the 21 ka SSTs reconstruction directly as in the GEN2 and UGAMP models [*Pinot et al.*, 1999], and not superimposing the change in SSTs between LGM and PD as given by *CLIMAP Project members* [1981] on the modern SSTs climatology. However, we do not think that the results will be greatly influenced by these two factors, especially at the resolution of the model, which is relatively coarse. Details of the paleovegetation and the continental ice experiments are provided in sections 5.1 and 5.2, respectively.

[13] All simulations are run for 12 years starting from the same initial atmospheric circulation conditions, and the results reported here are ensemble averages for the last 11 years. Here, we retain the modern calendar in our analysis of the results because the changes of the calendar at the LGM are negligible [*Levis et al.*, 1999]. Statistical significance is assessed by use of a student *t*-test (95% level) applied to differences between every two experiments where the standard deviation and degrees of freedom are based on the averages of the 11 individual years.

4. Simulation Results and Analysis

4.1. Climate Differences Between LGM and PD

[14] Simulated 21 ka climate differs greatly from that of PD (Figure 1 and Table 3). A global annual-average surface temperature decrease of 5.3°C is obtained, and the terrestrial temperature is reduced on average by 6.4°C at the LGM. Cooling is generally stronger over the Northern Hemisphere, and gradually decreases from the polar regions toward the tropics. At the same time, terrestrial cooling generally surpasses oceanic cooling in tropics. Cooling is very significant within the 60°N–90°N band with annual-average temperatures about 8–20°C below the PD values. The cooling maximum is located over the Norwegian Sea where the surface temperature is 18–20°C lower than at present. A secondary cooling maximum (exceeding 16°C) is located around the Aleutian Islands, which is possibly linked to the existence of a land bridge at the LGM at the current Bering Strait. Terrestrial surface temperature is lowered on average by 6.4°C at 30°N–60°N. Tropical Africa cools by 2–3°C, and Central America cools by 2°C or so. Although cooling is relatively weaker in the Southern Hemisphere, terrestrial surface temperature decreases on average by 7.8°C at 60°S–90°S. Annual-average temperature is 3–5°C lower in central and north China. Compared with the general global cooling, weak positive temperature anomalies appear over part of the Pacific, which can be attributed to the slightly warmer reconstructed *CLIMAP Project members* [1981] SSTs compared with the PD.

[15] As can be seen in Figure 1b and Table 3, drier climate dominated at the LGM. Global annual-average precipitation is down by 9%, and terrestrial precipitation accounts for only 71% of the present value. The reduction in precipitation is most profound from south China to Australia, with a value as much as −3 mm/day. As suggested by *Kutzbach et al.* [1998], this precipitation reduction can be attributed to the weakened Asian summer monsoon at the

Table 2. Boundary Conditions For Four Different Numerical Experiments

Experiment	Earth's Orbital Parameters	CO_2 Concentration, ppmv	SSTs, Sea Ice	Ice sheets, Topography and Coastline	Vegetation
Exp1	PD	345	PD	PD	PD
Exp2	LGM	200	*CLIMAP Project members* [1981]	*Peltier* [1994]	PD
Exp3	LGM	200	*CLIMAP Project members* [1981]	*Peltier* [1994]	replace current vegetation with that at the LGM over China
Exp4	LGM	200	*CLIMAP Project members* [1981]	*Peltier* [1994]	as in Exp 3, but replace vegetation with continental ice over part of the Tibetan Plateau

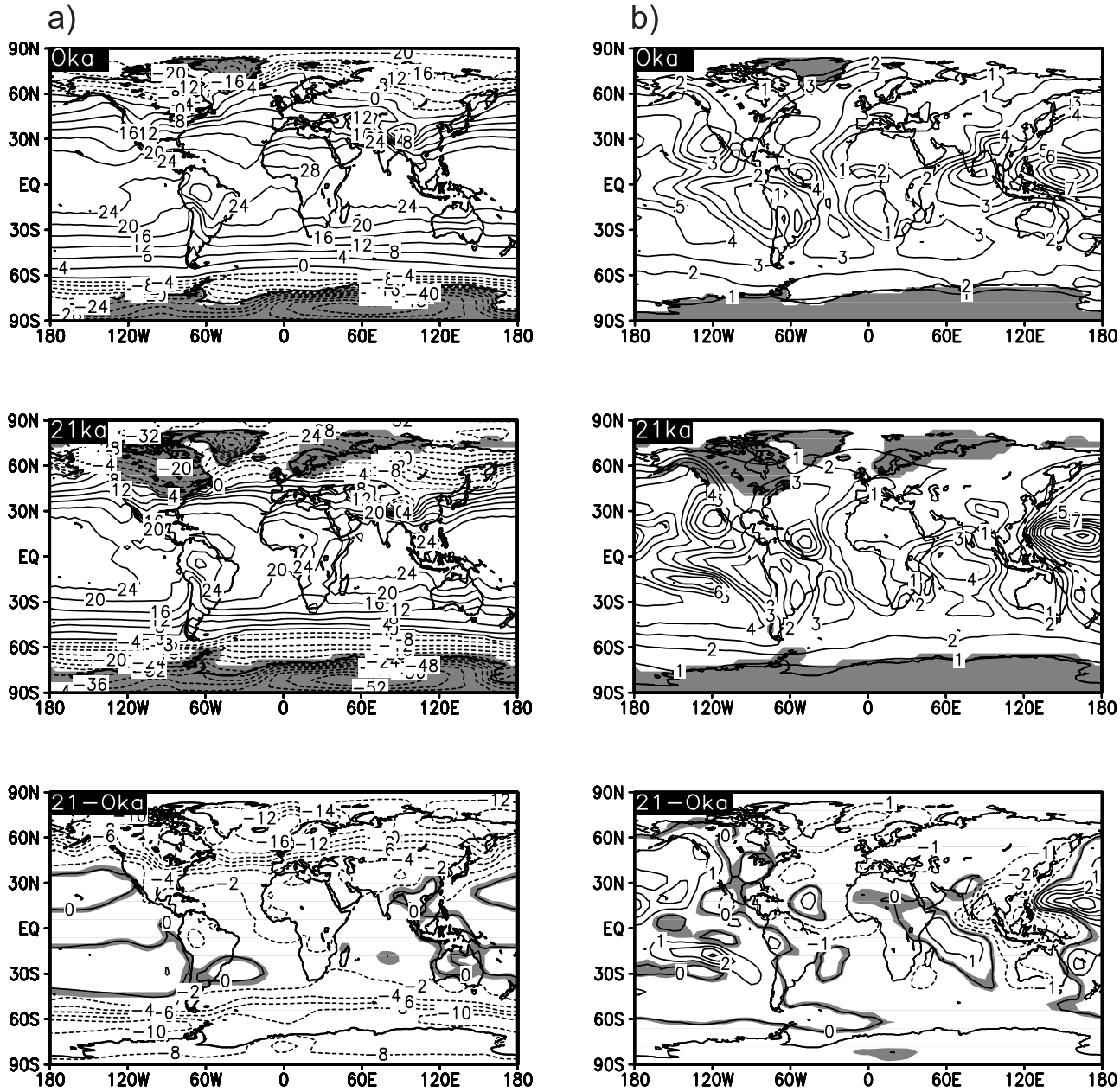

Figure 1. (a) Annual-average surface temperature in °C and (b) precipitation in mm/day (0 for PD, 21 for LGM, and 21-0 for LGM minus PD). The location of ice sheets is shaded in the upper four panels. The areas without the 95% confidence level are shaded in the lower two panels.

LGM (Figure 2). Precipitation reduction is relatively weak (only −0.5 mm/day or so) in the equatorial zone of the Americas, western Africa, and continental Eurasia. In contrast, wetter climate occurs in western North America, in the Andean Altiplano and over Arabia. *Thompson et al.* [1993] and *Harrison et al.* [1996] ascribed the wetter conditions in western North America to the southward displacement of the Northern Hemisphere westerly belt caused by the Laurentide Ice Sheet. In IAP-AGCM, wetter conditions over the above three regions can be attributed to the wind anomalies inland at 850 hPa (Figure 2). The precipitation increase over part of the western Pacific at the LGM is

Table 3. Land Surface Temperature (°C) and Precipitation Changes in Selected Latitude Bands[a]

Variables	90°N–60°N	60°N–30°N	30°N–0°N	0°–30°S	30°S–60°S	60°S–90°S	Global
Temperature (21-0)	−11.6	−6.4	−2.2	−1.0	−1.3	−7.8	−6.4
Precipitation (21/0)	64%	79%	61%	76%	98%	57%	71%

[a]In first column, 21-0 represents values of LGM minus PD, and 21/0 means fractional values of LGM relative to PD.

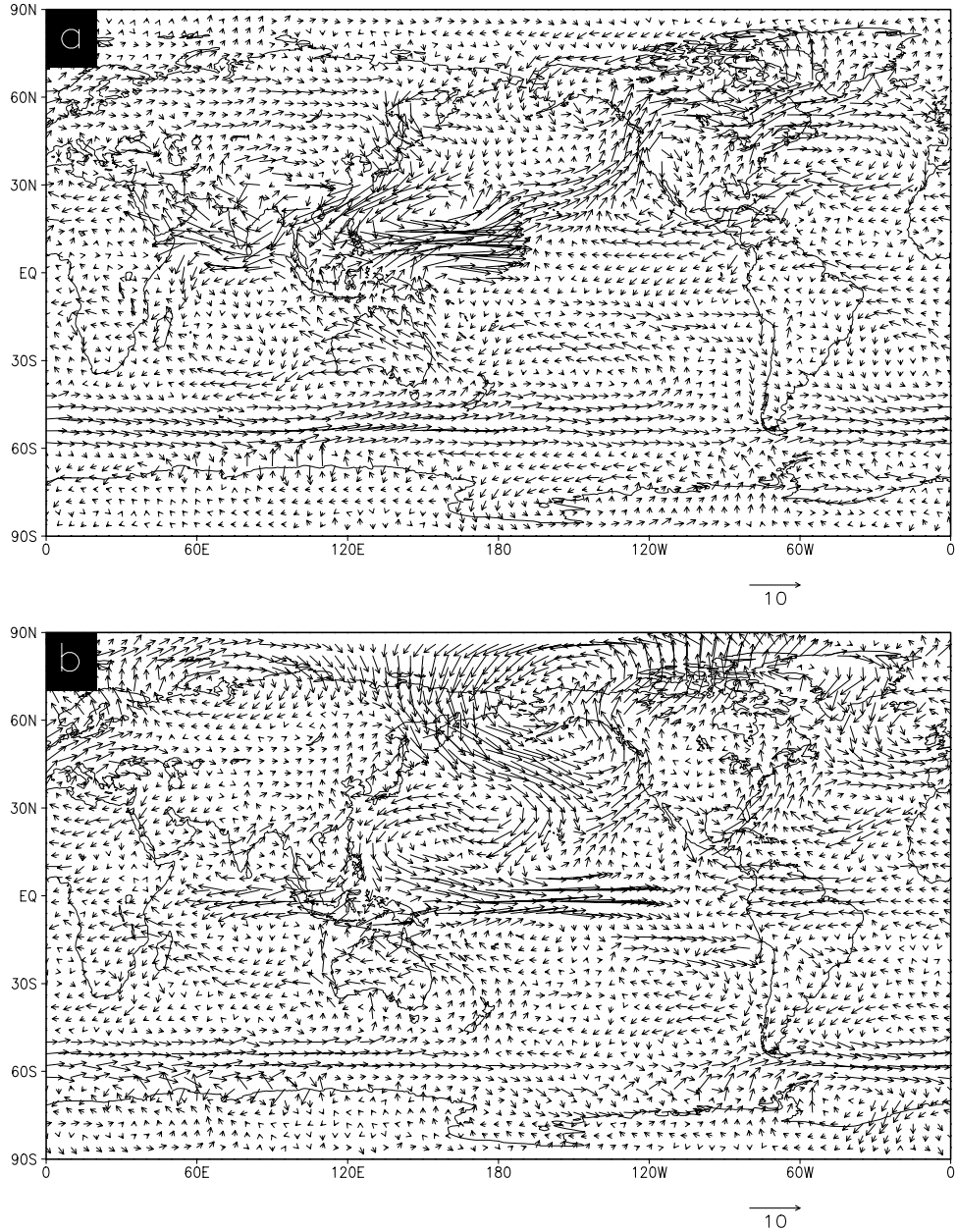

Figure 2. The 850-hPa wind differences between Exp2 and Exp1 in m/s for (a) boreal summer (JJA), and (b) boreal winter (DJF).

derived from a significantly anomalous cyclone located there, both in summer and winter (Figure 2).

4.2. Model-Model Comparison

[16] One of the PMIP goals is to identify common responses of AGCMs to the imposed glacial-age boundary conditions [*Joussaume and Taylor*, 1995]. So, it is of interest to compare our results with other PMIP model outputs. Here, we make use of the PMIP database (ftp://sprite.llnl.gov/./pub/pmip/database/) and compute zonally annual-average differences in surface temperature between LGM and PD simulated by PMIP fixed-SSTs AGCMs and IAP-AGCM. As shown in Figure 3, the colder 21 ka climate compared with PD is successfully reproduced by all of the AGCMs even if there are minor differences in the cooling magnitude. The IAP-AGCM outputs are generally in agreement with other PMIP fixed-SSTs AGCMs results. Furthermore, the geographical pattern of annual-average changes in surface temperature between LGM and PD from IAP-AGCM is also generally consistent with the average of all of the PMIP simulations using prescribed SSTs (for PMIP composite results, see *Joussaume and Taylor* [2000]). Largest disagreement is found in a region from south China to Australia where the temperature increases in IAP-AGCM. However, we also notice that temperature changes simulated by the PMIP fixed-SSTs AGCMs are in disorder, and exhibit great variability among the AGCMs in this region [*Pinot et al.*, 1999].

[17] Annual-average changes in precipitation between LGM and PD simulated by IAP-AGCM are also in agreement with the PMIP fixed-SSTs AGCMs results over the

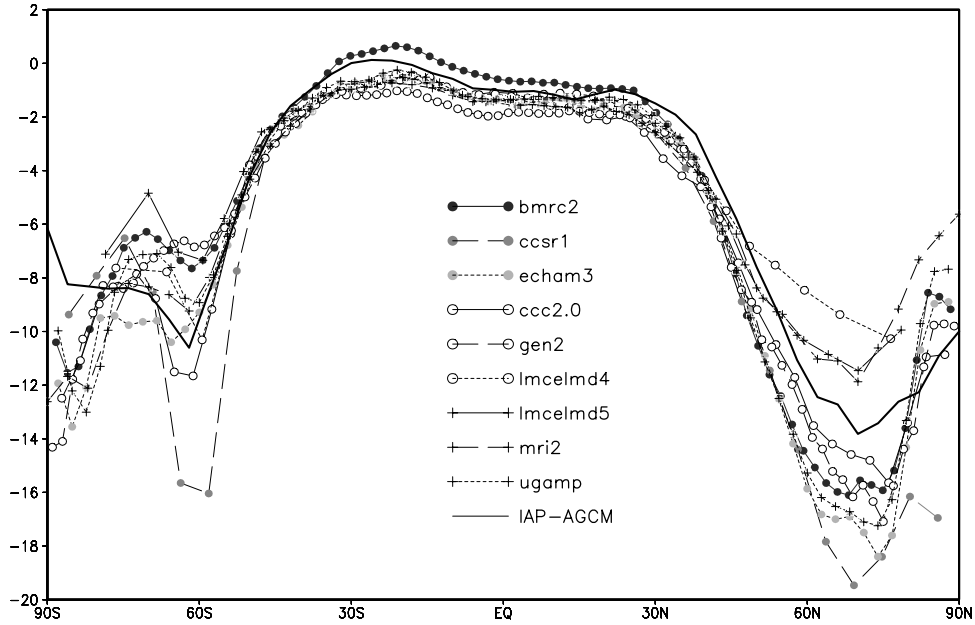

Figure 3. Zonally annual-average differences in surface temperature (°C) between LGM and PD simulated by the PMIP fixed-SSTs AGCMs and IAP-AGCM.

terrestrial and oceanic tropics (Table 4). At the same time, the simulated geographical pattern of the annual-average changes in precipitation by IAP-AGCM is also consistent with the composite results given by *Joussaume and Taylor* [2000]. We therefore conclude that IAP-AGCM reproduces the major characteristics of the 21 ka climate and can be used as a tool to study past climate changes.

4.3. Data-Model Comparison

[18] Using pollen, noble gas, plant macrofossils, speleothem, and lake status data, *Farrera et al.* [1999] derived a set of mutually consistent paleoclimate estimates of mean temperature of the coldest month (MTCO), mean annual temperature (MAT), plant available moisture (PAM), and runoff (P-E) in the 32°N–33°S latitude band for the LGM. Six regions listed in Table 5 are selected in this paper in order to compare IAP-AGCM outputs with proxy estimates, at the same time taking the error of data reconstruction and the interannual variability (represented by the standard deviation) of the simulated LGM climate into account. Here, we only give the values of MAT because of the minor differences between MAT and MTCO for the above regions based on the IAP-AGCM results. The table indicates the IAP-AGCM reproduces, to a certain degree, geographical cooling over the tropics. The model, however, generally underestimates the cooling magnitude reproduced from a variety of proxy data over all six regions. This is also a general weakness of the PMIP fixed-SSTs AGCM simulations. Logically, it reflects inadequacies of the reconstructed SSTs for the LGM [*CLIMAP Project members*, 1981] because the model-data disagreements are generally less in the PMIP computed-SSTs model [*Pinot et al.*, 1999]. As *Webster and Streten* [1978] and *Rind and Peteet* [1985] suggested, the small changes described by *CLIMAP Project members* [1981] for tropical SSTs in the Pacific and Indian Oceans are clearly an obstacle for the AGCM simulation of terrestrial cooling. Model-data disagreement is substantial

Table 4. Changes in Annual-Average Precipitation (mm/day) Between LGM and PD Simulated by Eight PMIP Fixed-SSTs AGCMs [*Pinot et al.*, 1999] and IAP-AGCM over Terrestrial and Oceanic Tropics (30°N–30°S)

Models With Prescribed SSTs	Precipitation Over Ocean	Precipitation Over Land
CCSR1	0.01	−0.14
ECHAM3	0.10	−0.50
GEN2	0.14	−0.65
LMD4	0.13	−0.47
LMD5	0.01	−0.30
LMDH	−0.19	−0.17
MR12	0.08	−0.58
UGAMP	0.00	−0.54
IAP-AGCM	**0.02**	**−0.32**

Table 5. Changes in Surface Temperature (°C) Between LGM and PD From Proxy Estimates, and IAP-AGCM[a]

	Proxy estimate (LGM minus PD)					IAP-AGCM		
	MTCO						SD	
Regions	Min	Max	Error	MAT	Error	MAT	Exp1	Exp2
A	−7.5	−15.5		−4	20–50%	−3.50	0.33	0.44
B				−5	20–50%	−2.53	0.38	0.47
C	−3	−6	20–50%			−1.81	0.25	0.33
D	−3.7	−6.5	20–50%	−5.5	20–50%	−1.40	0.35	0.27
E	−3	−5	20–50%			−2.59	0.25	0.16
F				−9	±2	−3.54	0.22	1.02

[a]SD means the standard deviation of mean annual surface temperatures simulated by IAP-AGCM in the following six regions. A: Eastern North America (75°W–85°W, 30°N–38°N), B: Western North America (95°W–115°W, 30°N–38°N), C: Northern South America (50°W–75°W, 10°N–2°S), D: South Africa (15°E–35°E, 18°S–30°S), E: Equatorial eastern Africa (25°E–40°E, 2°N–10°S), and F: the Tibetan Plateau (80°E–100°E, 30°N–38°N) (*Farrera et al.* [1999]; for the Tibetan Plateau, see *Shi et al.* [1997], *Yao et al.* [1998], and *Liu et al.* [1999]).

Table 6. Data-Model Comparison in Four Regions[a]

	Regions			
MAT (in °C)	A	B	C	D
Proxy estimates	−5 to −10	−5 to −10	−7 ± 3.5	−9 ± 2
Exp2-Exp1	−3.65	−1.76	0.23	−3.54
Exp3-Exp2	−0.14	−0.32	−0.50	−0.34
Exp4-Exp3	0.79	−0.37	0.08	−4.54

[a]A: Northeast China (120°E–130°E, 38°–50°N), B: Mideastern China (100°E–120°E, 30°N–42°N), C: South China (105°E–120°E, 22°N–30°N), D: the Tibetan Plateau (80°E–100°E, 30°N–38°N). For A and B, see *Yu et al.* [2001b]; for C, see *Farrera et al.* [1999]; for D, see Table 5.

over mainland China (Table 6), especially over south China and the Tibetan Plateau where simulated cooling (−3.54°C) is much smaller than the reconstructed one (−9°C). These disagreements cannot be reconciled under the boundary conditions from the framework of PMIP and motivate us to perform sensitivity experiments.

[19] The bioclimate variable PAM approximates the controls on vegetation more closely than the more conventional parameters of precipitation. It can be used to compare the simulated changes in mean annual precipitation [*Pinot et al.*, 1999]. According to the results of *Farrera et al.* [1999], the changes in PAM and P-E were both positive in western North America and on the Andean Altiplano at the LGM. In contrast, they were both negative in the equatorial zone of the Americas, western Africa and in Australia. The IAP-AGCM outputs are in agreement with these robust features. Pollen data indicate that the 21 ka climate is drier over the Tibetan Plateau. On the contrary, lake-level reconstruction shows higher lake levels, implying positive precipitation anomalies. In IAP-AGCM, most parts of mainland China is drier at the LGM compared with the PD, especially in east and south China. However, weak positive precipitation anomalies exist in the area from the western Tibetan Plateau to the southeastern Arabian Sea.

5. Sensitivity Experiments

5.1. Role of Paleovegetation Feedback Over China

[20] Vegetation influences the climate, primarily through its effect on albedo, evaporation, transpiration and roughness length. The resultant changes modify both the heat exchange and water vapor content of the atmosphere [*Wyputta and McAvaney*, 2001]. The drier-colder glacial-age climate at the LGM is quite different from that at the PD. Climate differences must lead to changes in the surface vegetation. In return, the 21 ka climate will change in response to vegetation changes. This section focuses on the role of vegetation feedback on the LGM climate over mainland China.

[21] Previously, two vegetation reconstructions for the LGM have been presented in the works of *Crowley* [1995] and *Adams and Faure* [1997]. They diverge greatly over many regions and imply uncertainty in the 21 ka vegetation. However, both of them are mainly characterized by an increase of desert areas in west China and savanna and semidesert in the other parts of China. In this study, the 21 ka vegetation over mainland China from *Yu et al.* [2000, 2001b] is applied. After manually converting the original data from 1° × 1° to 5° × 4° grid points in the region between 22°N–54°N and 75°E–135°E, it is found that the desert proportion expands in west China and short grassland, meadow, and shrubland spreads eastward at the expense of current dense vegetation (Figure 4). So, all three reconstructions confirm the enhancement of desert areas and sparse vegetation in response to the well-known colder-drier climate at the LGM in the selected areas even if some differences exist among them, for instance, desert areas and vegetation category. Besides vegetation change, soil color index associated with surface vegetation is also found to change in this study. The influence of the 21 ka vegetation on the regional climate was then examined.

[22] Vegetation substitution has a great impact on the simulation results (Figure 5). Two cooling centers appear in east and west China, respectively, where annual-average temperature reduction exceeds 0.5°C (1.8°C over the center of the Tibetan Plateau). Additional cooling reaches 30% of the value of Exp2 minus Exp1 in east and south China. The temperature decrease over the above areas can be attributed to surface albedo changes (Figure 6) due to the vegetation changes from PD to LGM because the latter has higher-albedo vegetation than the former. For this reason, more solar radiation is reflected in Exp3, leading to lower surface

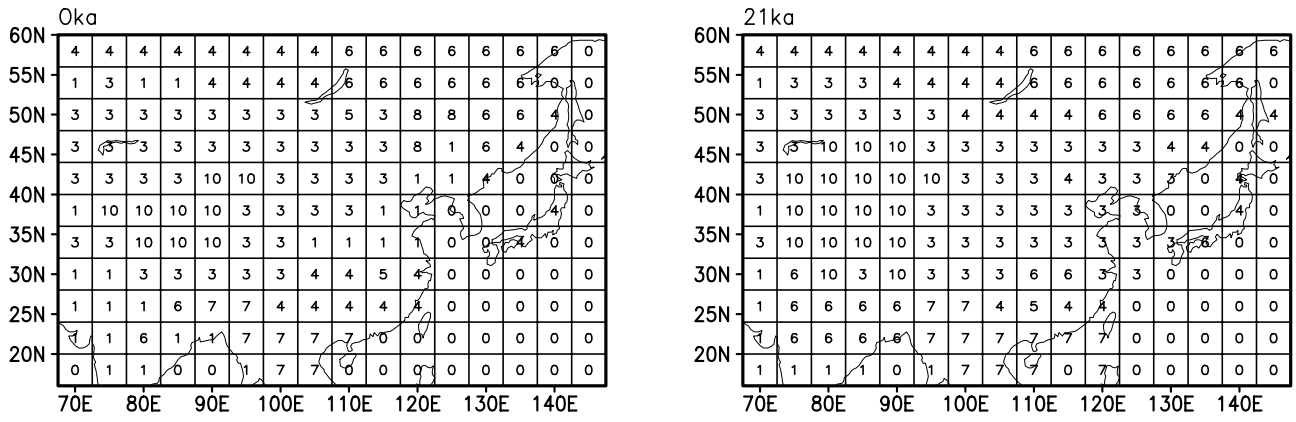

Figure 4. Surface vegetation in East Asia at 0 ka and 21 ka: 1, mixed farming, tall grassland; 2, tall/medium grassland, evergreen shrubland; 3, short grassland, meadow and shrubland; 4, evergreen forest (needle-leaved); 5, mixed deciduous, evergreen forest; 6, deciduous forest; 7, tropical evergreen broadleaved forest; 8, medium/tall grassland, woodlands; 9, tundra; 10, desert.

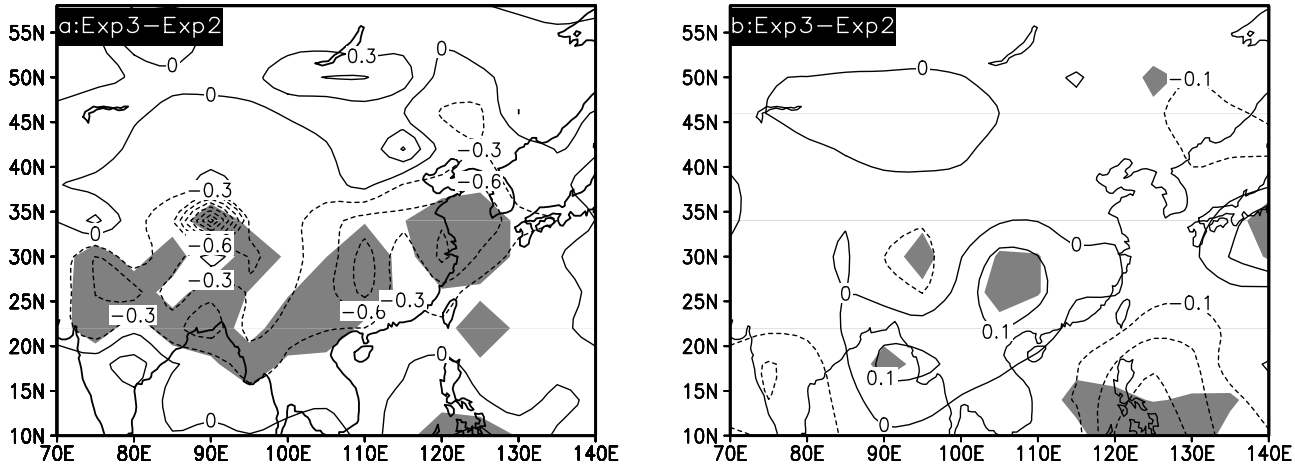

Figure 5. Climate changes (Exp3 minus Exp2) caused by paleovegetation over China for (a) temperature in °C and (b) precipitation in mm/day. The areas within the 95% confidence level are shaded.

temperature. As listed in Table 6, introducing 21 ka vegetation leads to additional cooling in four selected regions almost covering the whole mainland China and reduces regional temperature disagreements between the simulation results of Exp2 minus Exp1 and proxy estimates, especially in south China.

[23] The vegetation replacement also changes the regional precipitation field (Figure 5b). Precipitation increases by 0.1 mm/day in south China. Negative precipitation anomalies occur over the other parts of the mainland. For instance, precipitation decreases by 0.1 mm/day over part of the Tibetan Plateau. By comparing Figures 5 and 1, we can find that the influence of vegetation on precipitation is not so significant as the influence on temperature. In fact, the annual-average precipitation changes due to introduction of paleovegetation accounts for only 0–10% of that caused by the common 21 ka boundary conditions from PMIP over China.

5.2. Climate Response to the Continental Ice Over the Tibetan Plateau

[24] Controversies on the glacial-age environment over the Tibetan Plateau are well known [e.g., *Huntington*, 1906; *Kuhle*, 1987, 1991; *Han*, 1991; *Shi et al.*, 1997]. When *Kutzbach et al.* [1998] simulated the 21 ka climate with NCAR's CCM1 and BIOME (Version 1.0) model, a permanent small snowfield appeared over the Tibetan Plateau, and this phenomenon was attributed to the weakness of the India-South Asia monsoon at the LGM. It may imply that special changes occurred over this region at the LGM. *Liu et al.* [1999] studied the vegetation response to climate changes over China with a biome model named the "Taiji system," developed and validated by themselves. Results indicated that a large range of continental ice would appear over the Tibetan Plateau under a cooling of 5–9°C, even if moisture was kept constant. Moreover, they finally concluded that a large range of continental ice possibly existed there at the LGM. Recently, the same conclusion was reached when D. Jiang et al. (A further detection on the possibility of the existence of large-scale ice sheet over the Tibetan Plateau during the Last Glacial Maximum, submitted to *Chinese Journal of Atmospheric Sciences*, 2003) simulated the potential LGM vegetation distribution over China using the process-based equilibrium terrestrial biosphere model BIOME3 [*Haxeltine and Prentice*, 1996].

[25] With the debate still in progress, Exp4 is designed on the basis of Exp3 by replacing the 21 ka vegetation with continental ice over part of the Tibetan Plateau (30°N–34°N, 80°E–100°E [see *Liu et al.*, 1999]). In this way, the simulated influence of the continental ice feedback on the LGM climate can be evaluated.

[26] As shown in Figure 7, great changes in temperature and precipitation occur in response to the continental ice over part of the Tibetan Plateau. With the presence of continental ice, northeast China warms by 1°C or so. In contrast, annual-average temperature reduction surpasses 1°C, with a maximum of −7°C in midwestern China. The above-mentioned additional cooling can be attributed to the great regional changes in albedo (Figure 8a) due to the existence of continental ice. If one considers all of the boundary conditions of Exp4, surface temperature will

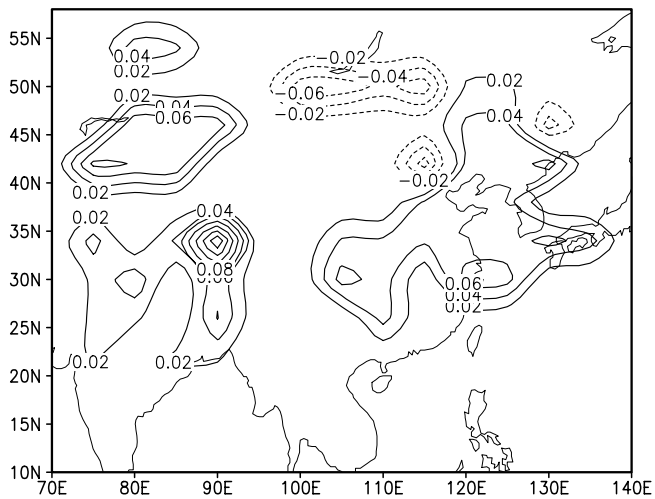

Figure 6. Annual-average anomalies (Exp3 minus Exp2) of albedo.

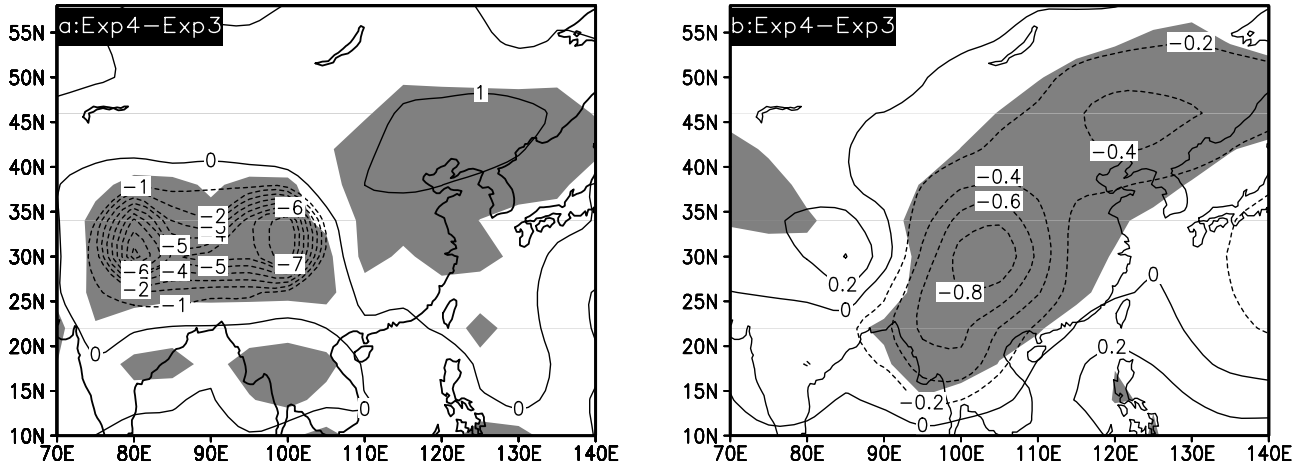

Figure 7. Climate changes (Exp4 minus Exp3) caused by the continental ice over part of the Tibetan Plateau for (a) temperature in °C and (b) precipitation in mm/day. The areas within the 95% confidence level are shaded.

decrease by 7–11°C over the Tibetan Plateau (Table 6). This value is in good agreement with the measurement from ice core measurements [*Yao et al.*, 1997] and other proxy estimates [*Shi et al.*, 1997; *Liu et al.*, 1999].

[27] The continental ice generally reduces regional precipitation, by as much as 30% relative to the value of Exp3 minus Exp1. The existence of continental ice over part of the Tibetan Plateau induces great regional cooling, which consequently leads to a strong anomalous anticyclone (Figure 8b) located over the Tibetan Plateau in summer. The anticyclone decreases the intensity of the East Asian summer monsoon, it shifts the subtropical high system over the western Pacific southeastward, and finally it leads to reduced precipitation over mideast China. In addition, a positive precipitation anomaly of 0.2 mm/day dominates over the western Tibetan Plateau. Based on Exp4, it follows that the glacial-age environment over the Tibetan Plateau is a very important factor for the 21 ka climate simulation. If the precondition of Exp4 is proved to be reliable, the influence of the continental ice on the 21 ka climate simulation will be decisive in East Asia.

6. Summary

[28] The climate response to the boundary conditions appropriate for the LGM, and the roles of paleovegetation cover over China and continental ice over part of the Tibetan Plateau, are studied using the IAP-AGCM with prescribed SSTs. The primary conclusions are as follows:

1. At the LGM, the global annual-average surface temperature decreased by 5.3°C, while terrestrial temperature reduction reached 6.4°C compared with the PD. The cooling gradually decreased from the polar regions toward the tropics, and was larger in the Northern Hemisphere. Moreover, terrestrial cooling generally surpassed oceanic cooling in tropics.

2. Drier climate dominated at the LGM. Global annual-average precipitation was found to be 91% of the present value. Terrestrial precipitation accounted for only 71% of the present value. In contrast, wetter conditions were

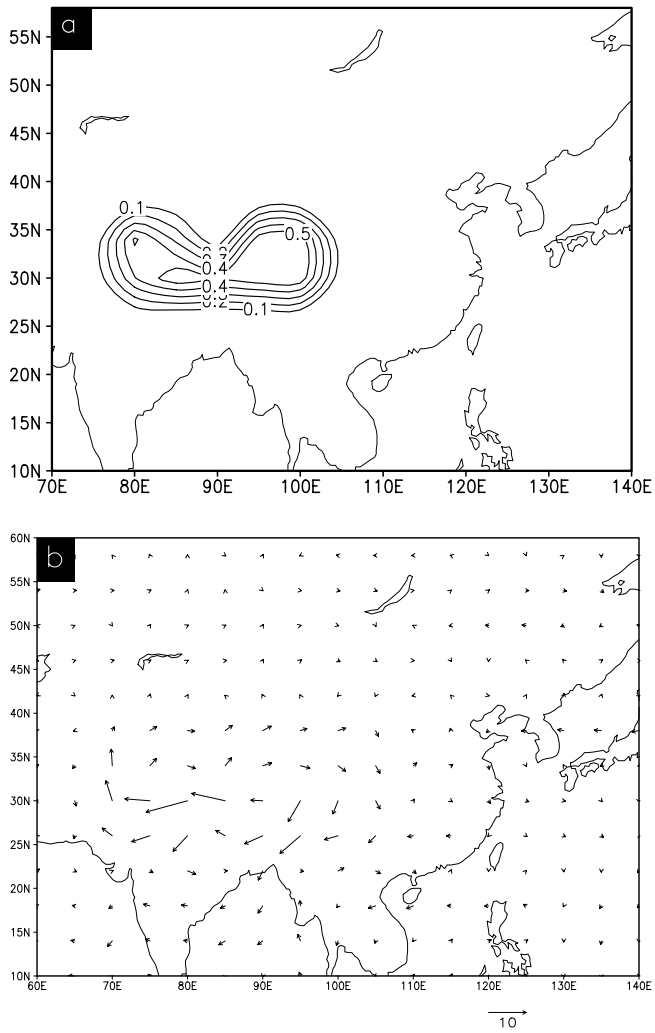

Figure 8. Annual-average anomalies (Exp4 minus Exp3) of (a) albedo, and (b) summer (JJA) 850-hPa wind differences in m/s.

registered in western North America, in Arabia, and over the Andean Altiplano.

3. Additional cooling due to the changes in vegetation and associated soil characteristics generally reduces, to a certain degree, model-data discrepancies over China.

4. Study of the role of continental ice feedback over the Tibetan Plateau indicates that if continental ice indeed existed at the LGM, its influence on the 21 ka climate would be very distinct in East Asia.

[29] The PMIP database provides us a unique opportunity to compare the model's response to the LGM boundary conditions with the proxy estimates. Because all of the PMIP fixed-SSTs AGCMs and the IAP-AGCM have underestimated the cooling over China, the role of 21 ka paleovegetation is addressed in this study. Even though subject to large uncertainty, vegetation reconstructions for the LGM are characterized by an increase of desert and sparse vegetation due to the drier-colder glacial-age climate over China. Based on this study and the works of *Crowley and Baum* [1997], *Kubatzki and Claussen* [1998], *Levis et al.* [1999], and *Wyputta and McAvaney* [2001], it follows that the role of vegetation feedback cannot be neglected if one aims for simulating the LGM climate. So, it is also necessary for PMIP members to choose a common vegetation reconstruction to evaluate the fixed-SSTs models' response to this missing glacial-age boundary condition.

[30] Also, our results confirm the conclusion reached by *Rind and Peteet* [1985] and *Pinot et al.* [1999] that it is difficult to reconcile the *CLIMAP Project members* [1981] SSTs reconstruction with terrestrial evidence. Several recent studies have suggested that the CLIMAP estimates are too warm, perhaps by several degrees, in the tropical ocean [e.g., *Guilderson et al.*, 1994; *Anderson and Webb*, 1994; *Webb et al.*, 1997; *Sonzogni et al.*, 1998]. The warmer CLIMAP SSTs may contribute to the inconsistency of the data-model comparisons over mainland China.

[31] Half of the PMIP models have been coupled to a slab ocean model with the hypothesis that the ocean meridional heat fluxes act similarly between LGM and PD. In fact, no one knows the meridional heat fluxes at the LGM. Furthermore, a slab ocean model neglects the differences in oceanic circulation at the LGM, which has been indicated in the works of *Ganopolski et al.* [1998] and *Weaver et al.* [1998]. However, the role of paleovegetation in the computed-SSTs models remains interesting.

[32] In addition, increased dust levels [e.g., *Petit et al.*, 1990] certainly change the radiation balance and consequently impact the climate system at the LGM. As put forward by *Kageyama et al.* [2001], dust is certainly a missing mechanism in the PMIP simulations and considerable development is required before its effects can be included in AGCMs. Even if the role of dust is difficult to evaluate [*Harrison et al.*, 2001], it must be done in order to obtain more reasonable LGM climate simulations in the future.

[33] **Acknowledgments.** We thank G. Yu for providing reconstructed vegetation data in East Asia, and the three anonymous reviewers for their valuable comments. Thanks are due to Ola M. Johannessen, Yongqi Gao, Odd Helge Otterå, Feng Zhang, and all at the Nansen Center for work assistance. This research was jointly supported by the National Natural Science Foundation of China under grant 40125014, and by the Chinese Academy of Sciences under grant KZCX2-203.

References

Adams, J. M., and H. Faure, Palaeovegetation maps of the Earth during the Last Glacial Maximum, and the early and mid Holocene: An aid to archaeological research, *J. Arch. Sci.*, *24*, 623–647, 1997.

Albrecht, B. A., V. Ramanathan, and B. A. Boville, The effects of cumulus moisture transports on the simulation of climate with a general circulation model, *J. Atmos. Sci.*, *43*, 2443–2462, 1986.

Anderson, D. M., and R. S. Webb, Ice-age tropics revisited, *Nature*, *367*, 23–24, 1994.

Arakawa, A., and W. H. Schubert, Interaction of a cumulus cloud ensemble with the large-scale environment, I, *J. Atmos. Sci.*, *31*, 674–701, 1974.

Barnola, J. M., D. Raynaud, Y. S. Korotkevich, and C. Lorius, Vostok ice core provides 160,000-year record of atmospheric CO_2, *Nature*, *329*, 408–414, 1987.

Berger, A. L., Long-term variations of daily insolation and quaternary climatic changes, *J. Atmos. Sci.*, *35*, 2362–2367, 1978.

Bi, X. Q., IAP 9-level atmospheric general circulation model and climate simulation, Ph.D. thesis, Inst. of Atmos. Phys., Chin. Acad. of Sci., Beijing, 1993.

Broccoli, A. J., Tropical cooling at the Last Glacial Maximum: An atmosphere-mixed layer ocean model simulation, *J. Clim.*, *13*, 951–976, 2000.

Broccoli, A. J., and S. Manabe, The influence of continental ice, atmospheric CO_2, and land albedo on the climate of the last glacial maximum, *Clim. Dyn.*, *1*, 87–99, 1987.

CLIMAP Project members, Seasonal reconstructions of the Earth's surface at the Last Glacial Maximum, *Map Chart Ser. MC-36*, Geol. Soc. of Am., Boulder, Colo., 1981.

COHMAP members, Climatic changes of the last 18,000 years: Observations and model simulations, *Science*, *241*, 1043–1052, 1988.

Crowley, T. J., Ice age terrestrial carbon changes revisited, *Global Biogeochem. Cycles*, *9*, 377–389, 1995.

Crowley, T. J., and S. K. Baum, Effect of vegetation on an ice-age climate model simulation, *J. Geophys. Res.*, *102*, 16,463–16,480, 1997.

Dong, B. W., and P. J. Valdes, Simulations of the Last Glacial Maximum climates using a general circulation model: Prescribed versus computed sea surface temperatures, *Clim. Dyn.*, *14*, 571–591, 1998.

Dong, B. W., P. J. Valdes, and N. M. J. Hall, The changes of monsoonal climates due to Earth's orbital perturbations and ice age boundary conditions, *Paleoclim. Data Modell.*, *1*, 203–240, 1996.

Farrera, I., et al., Tropical climates at the Last Glacial Maximum: A new synthesis of terrestrial palaeoclimate data, I, Vegetation, lake-levels and geochemistry, *Clim. Dyn.*, *15*, 823–856, 1999.

Ganopolski, A., S. Rahmstorf, V. Petoukhov, and M. Claussen, Simulation of modern and glacial climates with a coupled global model of intermediate complexity, *Nature*, *391*, 351–356, 1998.

Guilderson, T. P., R. G. Fairbanks, and J. L. Rubenstone, Tropical temperature variations since 20,000 years ago: Modulating interhemispheric climate change, *Science*, *263*, 663–665, 1994.

Han, T. L., *Large Ice Sheets Over the Tibetan Plateau*, 109 pp., China Geol., Beijing, 1991.

Harrison, S. P., G. Yu, and P. E. Tarasov, The late Quaternary lake-level records from northern Eurasia, *Quat. Res.*, *45*, 138–159, 1996.

Harrison, S. P., K. E. Kohfeld, C. Roelandt, and T. Claquin, The role of dust in climate changes today, at the Last Glacial Maximum and in the future, *Earth Sci. Rev.*, *54*, 43–80, 2001.

Haxeltine, A., and I. C. Prentice, BIOME3: An equilibrium terrestrial biosphere model based on ecophysiological constraints, resource availability, and competition among plant functional types, *Global Biogeochem. Cycles*, *10*, 693–709, 1996.

Huntington, E., Pangong: A glacial lake in the Tibetan Plateau, *J. Geol.*, *14*, 599–617, 1906.

Joussaume, S., and K. E. Taylor, Status of the Paleoclimate Modeling Intercomparison Project (PMIP), in Proceedings of the First International AMIP Scientific Conference, edited by W. L. Gates, *WCRP-92, WMO/TD-732*, pp. 425–430, World Meteorol. Org., Geneva, 1995.

Joussaume, S., and K. E. Taylor, The Paleoclimate Modeling Intercomparison Project, in Proceedings of the Third PMIP Workshop, edited by P. Braconnot, *WCRP-111, WMO/TD-1007*, pp. 9–24, World Meteorol. Org., Geneva, 2000.

Joussaume, S., et al., Monsoon changes for 6000 years ago: Results of 18 simulations from the Paleoclimate Modeling Intercomparison Project (PMIP), *Geophys. Res. Lett.*, *26*, 859–862, 1999.

Kageyama, M., O. Peyron, S. Pinot, P. Tarasov, J. Guiot, S. Joussaume, and G. Ramstein, The Last Glacial Maximum climate over Europe and western Siberia: A PMIP comparison between models and data, *Clim. Dyn.*, *17*, 23–43, 2001.

Kiehl, J. T., R. J. Wolski, B. P. Briegleb, and V. Ramanathan, Documentation of radiation and cloud routines in the NCAR Community Climate

Model (CCM1), *NCAR Tech. Note NCAR/TN-288+IA*, Natl. Cent. for Atmos. Res., Boulder, Colo., 1987.
Kohfeld, K. E., and S. P. Harrison, How well can we simulate past climates? Evaluating the models using global palaeoenvironmental datasets, *Quat. Sci. Rev.*, *19*, 321–346, 2000.
Kubatzki, C., and M. Claussen, Simulation of the global bio-geophysical interactions during the Last Glacial Maximum, *Clim. Dyn.*, *14*, 461–471, 1998.
Kuhle, M., Subtropical mountain- and highland-glaciation as ice age triggers and the waning of the glacial periods in the Pleistocene, *GeoJournal*, *14*, 393–428, 1987.
Kuhle, M., Observations supporting the Pleistocene inland glaciation of High Asia, *GeoJournal*, *25*, 133–231, 1991.
Kutzbach, J., R. Gallimore, S. Harrison, P. Behling, R. Selin, and F. Laarif, Climate and biome simulations for the past 21,000 years, *Quat. Sci. Rev.*, *17*, 473–506, 1998.
Leuenberger, M., and U. Siegenthaler, Ice-age atmospheric concentration of nitrous oxide from an Antarctic ice core, *Nature*, *360*, 449–451, 1992.
Levis, S., J. A. Foley, and D. Pollard, CO_2, climate, and vegetation feedbacks at the Last Glacial Maximum, *J. Geophys. Res.*, *104*, 31,191–31,198, 1999.
Liang, X. Z., Description of a nine-level grid point atmospheric general circulation model, *Adv. Atmos. Sci.*, *13*, 269–298, 1996.
Liu, T. S., X. S. Zhang, S. F. Xiong, and X. G. Qin, Qinghai-Xizang Plateau glacial environment and global Cooling, *China Quat. Sci.*, *5*, 385–396, 1999.
Lord, S. J., Development and observational verification of a cumulus cloud parameterization, Ph.D. thesis, Univ. of California, Los Angeles, Los Angeles, 1978.
Lord, S. J., W. C. Chao, and A. Arakawa, Interaction of a cumulus cloud ensemble with the large-scale environment, IV, The discrete model, *J. Atmos. Sci.*, *39*, 104–113, 1982.
Palmer, T. N., G. J. Shutts, and R. Swinbank, Alleviation of a systematic westerly bias in general circulation and numerical weather prediction models through an orographic gravity wave drag parameterization, *Q. J. R. Meteorol. Soc.*, *112*, 1001–1039, 1986.
Peltier, W. R., Ice age paleotopography, *Science*, *265*, 195–201, 1994.
Petit, J. R., L. Mounier, J. Jouzel, Y. S. Korotkevich, V. I. Kotlyakov, and C. Lorius, Palaeoclimatological and chronological implications of the Vostok core dust record, *Nature*, *343*, 56–58, 1990.
Pinot, S., G. Ramstein, S. P. Harrison, I. C. Prentice, J. Guiot, M. Stute, and S. Joussaume, Tropical paleoclimates at the Last Glacial Maximum: Comparison of Paleoclimate Modeling Intercomparison Project (PMIP) simulations and paleodata, *Clim. Dyn.*, *15*, 857–874, 1999.
Raynaud, D., J. Jouzel, J. M. Barnola, J. Chappellaz, R. J. Delmas, and C. Lorius, The ice record of greenhouse gases, *Science*, *259*, 926–934, 1993.
Rind, D., and D. Peteet, Terrestrial conditions at the Last Glacial Maximum and CLIMAP sea-surface temperature estimates: Are they consistent?, *Quat. Res.*, *24*, 1–22, 1985.
Sellers, P. J., Y. Mintz, Y. C. Sud, and A. Dalcher, A simple biosphere model (SiB) for use within general circulation models, *J. Atmos. Sci.*, *43*, 505–531, 1986.
Shi, Y. F., B. X. Zheng, and T. D. Yao, Glaciers and environments during the Last Glacial Maximum (LGM) on the Tibetan Plateau, *J. Glaciol. Geocryol.*, *19*, 97–113, 1997.
Slingo, J. M., The development and verification of a cloud prediction scheme for the ECMWF model, *Q. J. R. Meteorol. Soc.*, *113*, 899–927, 1987.
Smolarkiewicz, P. K., and W. W. Grabowski, The multidimensional positive definite advection transport algorithm: Nonoscillatory option, *J. Comput. Phys.*, *86*, 355–375, 1990.
Sonzogni, C., E. Bard, and F. Rostek, Tropical sea-surface temperatures during the last glacial period: A view based on alkenones in Indian Ocean sediments, *Quat. Sci. Rev.*, *17*, 1185–1201, 1998.
Thompson, R. S., C. Whitlock, P. J. Bartlein, S. P. Harrison, and W. G. Spaulding, Climatic changes in the western United States since 18,000 yr B. P., in *Global Climates Since the Last Glacial Maximum*, edited by H. E. Wright Jr. et al., pp. 468–513, Univ. of Minn. Press, Minneapolis, 1993.
Weaver, A. J., M. Eby, A. F. Fanning, and E. C. Wiebe, Simulated influence of carbon dioxide, orbital forcing and ice sheets on the climate of the Last Glacial Maximum, *Nature*, *394*, 847–853, 1998.
Webb, R. S., D. H. Rind, S. J. Lehman, R. J. Healy, and D. Sigman, Influence of ocean heat transport on the climate of the Last Glacial Maximum, *Nature*, *385*, 695–699, 1997.
Webster, P. J., and N. A. Streten, Late quaternary ice age climates of tropical Australasia: Interpretations and reconstructions, *Quat. Res.*, *10*, 279–309, 1978.
Wyputta, U., and B. J. McAvaney, Influence of vegetation changes during the Last Glacial Maximum using the BMRC atmospheric general circulation model, *Clim. Dyn.*, *17*, 923–932, 2001.
Yao, T. D., L. G. Thompson, Y. F. Shi, D. H. Qin, K. Q. Jiao, Z. H. Yang, L. D. Tian, and E. Mosley-Thompson, Climatic records since the last interglacial from the GULIYA ice core (in Chinese), *Sci. China, Ser. D*, *27*, 447–452, 1997.
Yin, J. H., and D. S. Battisti, The importance of tropical sea surface temperature patterns in simulations of Last Glacial Maximum climate, *J. Clim.*, *14*, 565–581, 2001.
Yu, G., et al., Palaeovegetation of China: A pollen data-based synthesis for the mid-Holocene and Last Glacial Maximum, *J. Biogeogr.*, *27*, 635–644, 2000.
Yu, G., X. Chen, J. Liu, and S. Wang, Preliminary study on LGM climate simulation and the diagnosis for East Asia, *Chin. Sci. Bull.*, *46*, 364–368, 2001a.
Yu, G., B. Xue, J. Liu, X. Chen, and Y. Q. Zheng, *Lake Records from China and the Palaeoclimate Dynamics*, pp.102–104, China Meteorol. Press, Beijing, 2001b.
Zeng, Q. C., C. G. Yuan, X. H. Zhang, X. Z. Liang, and N. Ban, A global grid-point general circulation model, in *Collection of Papers Presented at the WMO/IUGG NWP Symposium*, pp. 421–430, J. Meteorol. Soc. of Japan, Tokyo, 1987.
Zhang, X. H., Dynamical framework of IAP nine-level atmospheric general circulation model, *Adv. Atmos. Sci.*, *7*, 66–77, 1990.

H. Drange, Nansen Environmental and Remote Sensing Center, Edvard Griegsvei 3a, Bergen N-5059, Norway. (helge.drange@nersc.no)

D. Jiang, X. Lang, and H. Wang, State Key Laboratory of Numerical Modeling for Atmospheric Sciences and Geophysical Fluid Dynamics (LASG), Institute of Atmospheric Physics, Chinese Academy of Sciences, P. O. Box 9804 LASG, Beijing 100029, China. (jiangdb@mail.iap.ac.cn; langxm@mail.iap.ac.cn; wanghj@mail.iap.ac.cn)